PERGAMON

International Journal of Heat and Mass Transfer 44 (2001) 2611–2619

International Journal of HEAT and MASS TRANSFER

www.elsevier.com/locate/ijhmt

Time-resolved spatial distribution of scattered radiative energy in a two-dimensional cylindrical medium with a large mean free path for scattering

Shang-Hsuang Wu, Chih-Yang Wu *

Department of Mechanical Engineering, National Cheng Kung University, Tainan, Taiwan 701, ROC

Received 21 January 2000; received in revised form 22 September 2000

Abstract

Transient radiative transfer in a 2-D finite cylindrical medium with collimated pulse irradiation and a large mean free path for scattering is considered thoroughly. Highly accurate solutions of integral equation for the transient radiative transfer reveal that the radiative energy of the medium core is less than the radiative energy of the medium boundary, after the attenuated pulse irradiation has passed through the medium. The distinction between the extraordinary results of the above case and the results of other cases is examined. It is found that influence of the decrease rate of radiative energy with the passage of time is larger than that of the extinction decay of the radiative intensity along a propagation path for transient radiative transfer in a 2-D medium with a large mean free path for scattering. Moreover, scattering coefficient and geometric size are the major factors determining the spatial distribution type of scattered radiation energy at large time and the temporal evolution of the spatial distribution type of radiation energy. © 2001 Published by Elsevier Science Ltd.

Keywords: Transient radiative transfer; Integral formulation; Large mean free path; Scattering; Monte Carlo method

1. Introduction

Scattering and propagation of light through a scattering medium exposed to a pulse irradiation is a topic of current interest. Examples are optical pulse diffusion in bio-tissues and optical properties estimation from time-resolved measurement of light [1,2]. When treating the transient radiative transfer analytically, diffusion and more rigorous approximation [2,3], Monte Carlo method [1,4] and numerical solutions of exact integral formulation [5,6] were developed. Since most studies on transient radiative transfer consider optically moderate and thick media, in this work great interests are focused on the time-resolved spatial distribution of radiative energy in an optically thin medium. Radiation propagation in optically thin media is considered in radar and communication engineering [7]. Basic information obtained from the study on the time dynamics of photon migration in random media for both small and large mean free paths of scattering will help in the development of ranging and 3-D imaging devices [8]. Recently, Pham and coworkers [9] have used frequency-domain planar photon density waves to determine optical properties of layered tissue-like media for various cases including optically thin ones.

Comparisons in Refs [5,6] show that the solutions of the integral formulation by a quadrature method (QM) are accurate, and so the approach is adopted here to investigate the transient radiative transfer in 2-D finite cylindrical media with collimated pulse irradiation. The results show that, if the medium has a very large mean free path for scattering (MFPS), the inverse of the scattering coefficient, as compared with its geometric size, the radiative energy of the medium near the boundary is more than that of the medium core, after the attenuated pulse irradiation has passed through the medium. To our best knowledge, such a phenomenon has not been reported yet. Therefore, the distinction between the extraordinary results of the above case and

* Corresponding author.

0017-9310/01/$ - see front matter © 2001 Published by Elsevier Science Ltd.
PII: S0017-9310(00)00306-9

Nomenclature

c	speed of light in the medium
$\mathbf{e}_r, \mathbf{e}_\psi, \mathbf{k}$	unit vectors in the r-, ψ- and z-directions, respectively, see Fig. 1
F	function describing the temporal shape of the irradiation, see Eq. (4)
I	radiation intensity
I_0	peak value of the pulse
M_{00}	incident radiation function
M_{10}, M_{11}	z- and r-components of radiative flux
N_φ, N_μ, N_s	quadrature point numbers for φ, μ and s integrations, respectively
r, ψ, z	cylindrical coordinates, see Fig. 1
r_0, z_0	radius and height of the cylindrical medium, respectively
s	distance measured from the point considered reversely along the direction denoted by θ and φ
t	time
t_c	time when the peak of the pulse enters the medium
t_p	full width at half maximum for F
u	radiation energy density

Greek symbols

β	extinction coefficient
ζ	function defined in Eq. (13)
θ	polar angle
κ	absorption coefficient
μ	$\cos\theta$
σ_s	scattering coefficient
φ	azimuthal angle
ω	scattering albedo

Subscripts

u	upper limit
w	boundary

the results of other cases is examined thoroughly in this work.

2. Formulation and numerical methods

Transient radiative transfer in an absorbing, isotropically scattering, 2-D axisymmetric finite cylindrical medium (radius r_0 and height z_0) is considered here. The medium is assumed to be cold; that is, the emission of the medium is negligibly small as compared with the irradiation at the medium boundary. The radiative properties of the medium are considered to be constant, and the scattering is instantaneous or of no retention time. The spatial and the directional coordinate systems are shown in Fig. 1. Both r_0 and z_0 are assumed to be much larger than the wavelength. Then, the radiative intensity I at a position denoted by r and z along a direction denoted by the polar angle, θ, and the azimuthal angle, φ, at time t can be described by the equation of transient radiative transfer

$$\frac{1}{c}\frac{\partial I(r,z,\mu,\varphi,t)}{\partial t} + (1-\mu^2)^{1/2}\cos\varphi\frac{\partial I(r,z,\mu,\varphi,t)}{\partial r} - \frac{(1-\mu^2)^{1/2}\sin\varphi}{r}\frac{\partial I(r,z,\mu,\varphi,t)}{\partial \varphi} + \mu\frac{\partial I(r,z,\mu,\varphi,t)}{\partial z} + \beta I(r,z,\mu,\varphi,t) = \frac{1}{4\pi}\sigma_s M_{00}(r,z,t), \tag{1}$$

where $\mu = \cos\theta$, c the speed of light in the medium, β the extinction coefficient, and σ_s is the scattering coefficient. The incident radiation function, M_{00}, is defined as

$$M_{00}(r,z,t) = \int_0^{2\pi}\int_{-1}^{1} I(r,z,\mu,\varphi,t)\,\mathrm{d}\mu\,\mathrm{d}\varphi, \tag{2}$$

and is related to the radiation energy density u through $M_{00}(r,z,t) = cu(r,z,t)$.

The medium is exposed to a spatially uniform collimated time-dependent irradiation normal to the circular bottom surface at $z = 0$, the top and lateral surfaces are free from irradiation, and the boundaries of the medium are not reflecting. The temporal shape of the irradiation is considered to be a pulse described by a truncated Gaussian distribution. Then, the boundary condition for Eq. (1) can be expressed as

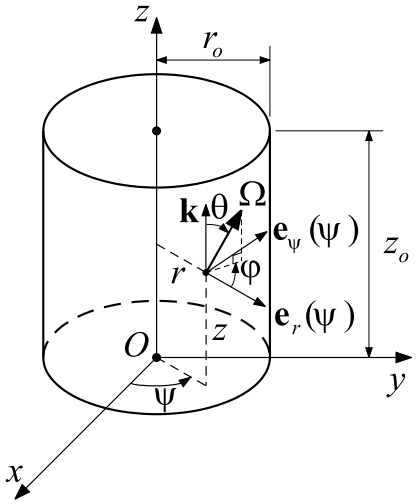

Fig. 1. The geometry and the coordinate systems.

$$I(r,0,\mu,\varphi,t) = I_0 F(t)\delta(\mu-1)\delta(\varphi) \quad \text{for } 0\leqslant r\leqslant r_0,\ \mu>0,\ 0\leqslant\varphi<2\pi,\ t\geqslant 0, \tag{3a}$$

$$I(r,z_0,\mu,\varphi,t) = 0 \quad \text{for } 0\leqslant r\leqslant r_0,\ \mu<0,\ 0\leqslant\varphi<2\pi,\ t\geqslant 0, \tag{3b}$$

$$I(r_0,z,\mu,\varphi,t) = 0 \quad \text{for } 0\leqslant z\leqslant z_0,\ -1\leqslant\mu\leqslant 1,\ \pi/2<\varphi<3\pi/2,\ t\geqslant 0, \tag{3c}$$

where δ is the delta function, and the function F is defined as

$$F(t) = \exp\left[-4(\ln 2)\left(\frac{t-t_c}{t_p}\right)^2\right] \tag{4}$$

with t_c denoting the time when the pulse reaches its maximum and t_p denoting the full width at half maximum (FWHM) for F. By changing the expression of F, the following integral formulation can be readily applied to a problem with other temporal shapes of irradiation. We assume that there is no radiation energy within the medium initially. Thus, the initial condition is

$$I(r,z,\mu,\varphi,0) = 0 \quad \text{for } 0\leqslant r\leqslant r_0,\ 0\leqslant z\leqslant z_0,\ -1\leqslant\mu\leqslant 1,\ 0\leqslant\varphi<2\pi. \tag{5}$$

The notation denoting the spectral dependence of the radiative properties has been omitted to simplify the mathematical formulation; the present equations are valid for monochromatic or gray radiative transfer.

Substituting the formal solution of intensity obtained from the integration of Eq. (1) into Eq. (2), we can obtain the integral equation of M_{00} [6]

$$M_{00}(r,z,t) = I_0 F(t-z/c)\exp(-\beta z)H(ct-z) + \frac{1}{4\pi}H(ct-z)\int_0^{2\pi}\int_{-1}^{1}\int_0^{s_u(r,z,\mu,\varphi,t)}\beta\omega \times \exp(-\beta s)\, M_{00}[r'(r,s,\mu,\varphi), z'(z,s,\mu), t-s/c]\,\mathrm{d}s\,\mathrm{d}\mu\,\mathrm{d}\varphi, \tag{6}$$

where H is the Heaviside step function, $\omega=\sigma_s/\beta$ the scattering albedo, and s the geometric distance from the considered point (r,z) to the scattering point (r',z') at which radiation is scattered at the instant $t'=t-s/c$ to contribute to the M_{00} at the considered point (r,z) at the instant t. The first and second terms on the right-hand side of Eq. (6) represent the driving term and the scattering contribution, respectively. In Eq. (6), we define

$$r'(r,s,\mu,\varphi) = [r^2 - 2rs(1-\mu^2)^{1/2}\cos\varphi + s^2(1-\mu^2)]^{1/2}, \tag{7}$$

$$z'(z,s,\mu) = z - s\mu, \tag{8}$$

$$s_u(r,z,\mu,\varphi,t) = \min\{(ct-z)/(1-\mu), s_w(r,z,\mu,\varphi)\}, \tag{9}$$

where $\min\{x,y\}$ denotes the smaller value of x and y and s_w is the distance from the considered point labeled by r and z to the nearest point on the medium boundary seen from the considered point reversely along the direction denoted by θ and φ. It is readily found that

$$s_w(r,z,\mu,\varphi) = \begin{cases} -(z_0-z)/\mu & \text{for } -1\leqslant\mu<\mu_1(r,z,\varphi), \\ \zeta(r,\varphi)/(1-\mu^2)^{1/2} & \text{for } \mu_1(r,z,\varphi)\leqslant\mu\leqslant\mu_2(r,z,\varphi), \\ z/\mu & \text{for } \mu_2(r,z,\varphi)<\mu\leqslant 1 \end{cases} \tag{10}$$

with

$$\mu_1(r,z,\varphi) = -\cos\{\arctan[\zeta(r,\varphi)/(z_0-z)]\}, \tag{11}$$

$$\mu_2(r,z,\varphi) = \cos\{\arctan[\zeta(r,\varphi)/z]\}, \tag{12}$$

$$\zeta(r,\varphi) = r\cos\varphi + (r_0^2 - r^2\sin^2\varphi)^{1/2}. \tag{13}$$

As shown in Eq. (6), s_u represents the length determining the domain of dependence of the M_{00} at the position (r,z). Since the domain of dependence of M_{00} may vary with time, Eq. (6) is a Volterra integral equation.

We also take interest in the z- and r-components of radiative flux, M_{10} and M_{11}, defined as

$$\begin{Bmatrix} M_{10}(r,z,t) \\ M_{11}(r,z,t) \end{Bmatrix} = \int_0^{2\pi}\int_{-1}^{1} I(r,z,\mu,\varphi,t) \times \begin{Bmatrix} \mu \\ (1-\mu^2)^{1/2}\cos\varphi \end{Bmatrix}\mathrm{d}\mu\,\mathrm{d}\varphi. \tag{14}$$

They can be expressed in terms of M_{00} as [6]

$$\begin{Bmatrix} M_{10}(r,z,t) \\ M_{11}(r,z,t) \end{Bmatrix} = I_0 F(t-z/c)\exp(-\beta z)\begin{Bmatrix} 1 \\ 0 \end{Bmatrix}H(ct-z) + \frac{1}{4\pi}H(ct-z) \times \int_0^{2\pi}\int_{-1}^{1}\int_0^{s_u(r,z,\mu,\varphi,t)}\beta\omega \times \exp(-\beta s) \times \begin{Bmatrix} \mu \\ (1-\mu^2)^{1/2}\cos\varphi \end{Bmatrix} \times M_{00}[r'(r,s,\mu,\varphi), z'(z,s,\mu), t-s/c] \times \mathrm{d}s\,\mathrm{d}\mu\,\mathrm{d}\varphi. \tag{15}$$

The method adopted to solve the integral equation of M_{00} is the QM; the details of the QM have been given in [5,6]. To validate the results obtained by the QM, we also solve the problem by the reverse (or backward) Monte Carlo method (RMCM) [10,11].

3. Results and discussion

To illustrate the extraordinary distribution of radiative energy for transient radiative transfer in a finite 2-D cylindrical medium with a large MFPS, we consider the cases with the aspect ratio $z_0/r_0 = 1.0$ and a pulse irradiation of $ct_c/z_0 = 1.0$ and $ct_p/z_0 = 0.33302$.

First, the accuracy of solutions obtained by the QM is examined for an optically thin case; the solutions obtained by the QM for transient radiative transfer in an optically moderate or thick medium have been shown to be accurate [6]. For comparison, results obtained by the RMCM as well as those by the QM are listed in Table. 1. To keep the statistical (or random) error inherent within the RMCM results small enough, 10^8 bundles are used to generate each RMCM result. The value just following each RMCM result in parentheses is the estimation of the standard deviation of the RMCM result. The standard deviation can be viewed as an indicator of the magnitude of random error within the result. We tabulate the results generated by using 21×21 and 41×41 uniform grid points with quadrature points $N_\varphi = N_\mu = 10$ and $N_s = 40$ (quadrature set A) to examine the grid-dependence of the QM results. To show the quadrature-dependence, another set of quadrature points, $N_\varphi = N_\mu = 7$ and $N_s = 30$ (quadrature set B), is also employed associated with the 41×41 grid mesh. In Table. 1, the number after the abbreviation "QM" represents the number of grids used, while the alphabet "A" or "B" indicates the quadrature set employed.

The QM and the RMCM which are quite different in essence generate consistent solutions for a long duration, as shown in Table. 1. Comparing the three sets of QM results tabulated in Table. 1, we find that the QM results converge very fast; the results generated by employing less grid and less quadrature points are very close to those by using the 41×41 grid mesh and quadrature set A. Moreover, the CPU time required by the QM with the 41×41 spatial grid points, 200 time steps and quadrature set A to solve the present example is about 4.51×10^4 s on a DEC Alpha 8400 computer, while that required by the RMCM to generate M_{00}, M_{10} and M_{11} on a 3×3 grid points at 6 instants is about 2.20×10^6 s. Therefore, the QM is not only accurate but also efficient.

Table 1 and the comparison in [6] show that the 21×21 grid mesh with quadrature set A and the 21×21 grid mesh with quadrature set B can generate accurate results for the optically thin and the optically moderate cases, respectively. Thus, they are employed to generate the plotted results in this work to save the CPU time required.

The graphic M_{00} results obtained by the QM for the above optically thin case are shown in Figs. 2 and 3 To exhibit the evolution of the time-resolved spatial distribution of radiative energy within the optically thin medium, results in series are presented in Figs. 2(a)–(f). Figs. 2(a) and (b) show the instantaneous spatial distributions of M_{00} when the peak of the unscattered penetrating irradiation reaches the $z = z_0/2$ and the $z = z_0$ planes, respectively. In the optically thin case, the unscattered penetrating irradiation is the main contribution to the M_{00} before the attenuated pulse irradiation passes through the medium. Since the spatial distribution of irradiation is independent of r, the M_{00} results on

Table 1
The results of M_{00} for a medium with $\beta r_0 = \beta z_0 = 0.1$ and $\omega = 1.0$ obtained by the QM and by the RMCM[a]

			$M_{00}(r,z,t)/I_0$			
r/r_0	z/z_0	ct/z_0	QM 21A	QM 41B	QM 41A	RMCM
0.0	0.0	2.0	0.011008	0.011009	0.011010	0.0110099 (1.7×10^{-7})
0.0	0.5	2.0	0.025810	0.025812	0.025812	0.0258138 (1.4×10^{-6})
0.0	1.0	2.0	0.926684	0.926684	0.926684	0.9266848 (1.3×10^{-6})
1.0	0.0	2.0	0.004644	0.004650	0.004644	0.0046461 (2.3×10^{-7})
1.0	0.5	2.0	0.011959	0.011970	0.011961	0.0119615 (7.3×10^{-7})
1.0	1.0	2.0	0.914983	0.914982	0.914985	0.9149878 (6.6×10^{-7})
0.0	0.0	3.0	0.003462	0.003476	0.003463	0.0034640 (3.7×10^{-7})
0.0	0.5	3.0	0.002207	0.002208	0.002208	0.0022083 (3.9×10^{-7})
0.0	1.0	3.0	0.001577	0.001577	0.001577	0.0015778 (2.0×10^{-7})
1.0	0.0	3.0	0.002844	0.002842	0.002844	0.0028451 (2.4×10^{-7})
1.0	0.5	3.0	0.002868	0.002864	0.002868	0.0028695 (5.0×10^{-7})
1.0	1.0	3.0	0.002983	0.002975	0.002983	0.0029823 (4.2×10^{-7})
0.0	0.0	5.0	1.983×10^{-6}	1.963×10^{-6}	1.974×10^{-6}	1.976×10^{-6} (2.4×10^{-9})
0.0	0.5	5.0	1.711×10^{-6}	1.698×10^{-6}	1.703×10^{-6}	1.704×10^{-6} (2.3×10^{-9})
0.0	1.0	5.0	2.204×10^{-6}	2.192×10^{-6}	2.196×10^{-6}	2.196×10^{-6} (2.8×10^{-9})
1.0	0.0	5.0	5.073×10^{-6}	5.056×10^{-6}	5.064×10^{-6}	5.065×10^{-6} (5.8×10^{-9})
1.0	0.5	5.0	4.516×10^{-6}	4.506×10^{-6}	4.509×10^{-6}	4.509×10^{-6} (7.2×10^{-9})
1.0	1.0	5.0	5.204×10^{-6}	5.191×10^{-6}	5.197×10^{-6}	5.202×10^{-6} (5.6×10^{-9})

[a] The value within the pair of parentheses is the estimation of the standard deviation of the RMCM results.

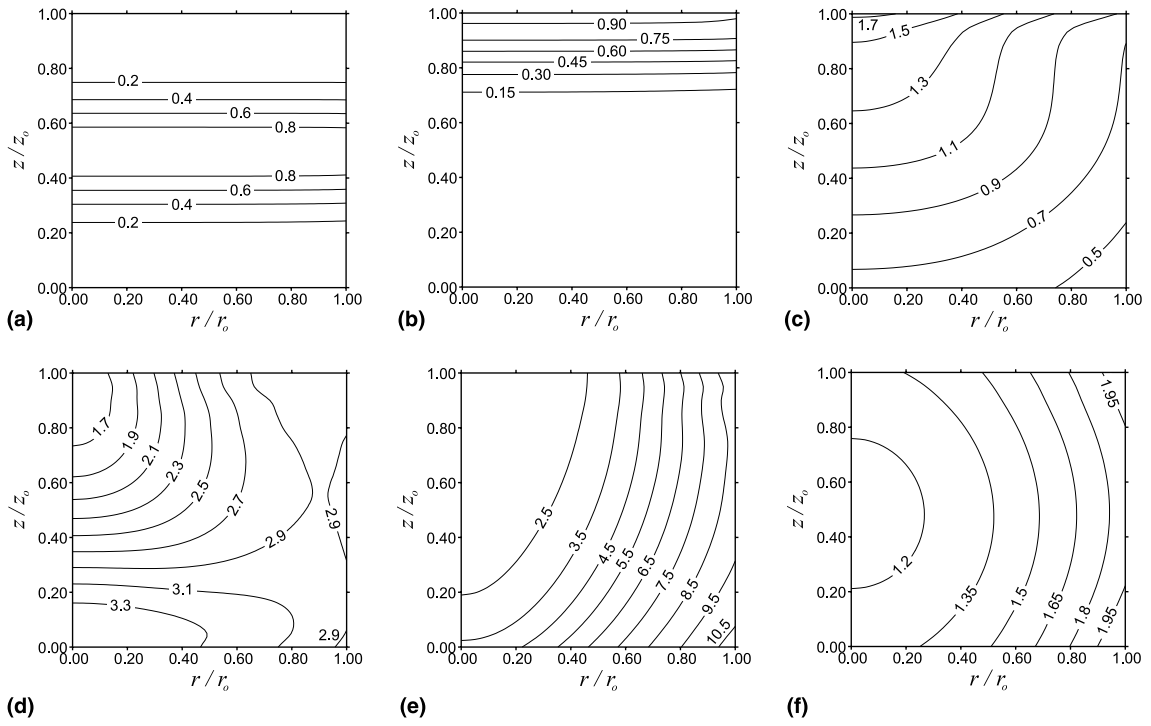

Fig. 2. The time-resolved spatial distribution of $M_{00}(r,z,t)$ for the case with $\beta r_0 = \beta z_0 = 0.1$ and $\omega = 1.0$: (a) M_{00}/I_0 at $ct/z_0 = 1.5$; (b) M_{00}/I_0 at $ct/z_0 = 2.0$; (c) $(M_{00}/I_0) \times 10^2$ at $ct/z_0 = 2.5$; (d) $(M_{00}/I_0) \times 10^3$ at $ct/z_0 = 3.0$; (e) $(M_{00}/I_0) \times 10^4$ at $ct/z_0 = 3.5$; (f) $(M_{00}/I_0) \times 10^5$ at $ct/z_0 = 4.5$.

a $z =$ constant plane exhibit a high uniformity at an instant before $ct/z_0 = 2.0$, as shown in Figs. 2(a) and (b). After the peak of the unscattered penetrating irradiation has reached the $z = z_0$ plane, the scattered radiation gradually becomes the dominant contribution to the M_{00}, and the magnitude of M_{00} decreases rapidly due to radiation loss from the medium boundary as t increases. Thus, the M_{00} near the lateral surface, $r = r_0$, becomes smaller than that around the symmetric axis, $r = 0$, as displayed in Fig. 2(c). At the instant, the location of the largest M_{00} appears around the point $(0, z_0)$.

At the early stage of the scattered-radiation-dominant period, the larger M_{00} in the region around the point $(0, z_0)$ plays a role similar to a diffuse radiative source, and the radiative energy of the source propagates nearly isotropically to other parts of the medium later. Fig. 2(d) shows that the spatial distribution of M_{00} at the instant $ct/z_0 = 3.0$. It is found that at the instant the region with a larger M_{00} shifts to the neighborhood of the bottom surface, $z = 0$, and the region with a larger M_{00} extends to the corner near to the point (r_0, z_0) along the bottom and the lateral surfaces. On the other hand, the smallest M_{00} appears around the point $(0, z_0)$ at the instant. At a later instant, $ct/z_0 = 3.5$, the M_{00} at the point $(r_0, 0)$ has the largest value, while the smallest M_{00} is located at the point $(0, z_0)$, as shown in Fig. 2(e). As time passes further, the location of the smallest M_{00} moves along the symmetric axis in the negative z-direction to the neighborhood of the central point $(0, z_0/2)$, and the regions near the two corner points, $(r_0, 0)$ and (r_0, z_0), have larger values of M_{00} than the other parts of the medium. This can be easily identified from Fig. 2(f), which displays the spatial distribution of M_{00} at $ct/z_0 = 4.5$. It is worth noting that after $ct/z_0 = 4.5$, at least during the period observed, $ct/z_0 \leqslant 30.0$, the distribution of M_{00} keeps to have a similar distribution to that at $ct/z_0 = 4.5$. An example of the instant $ct/z_0 = 10.0$ is shown in Fig. 3.

Based on intuition, one might not accept that the M_{00} of the medium core is less than the M_{00} of the medium boundary, where radiative energy can readily escape from the medium. However, the present results do show such distributions of M_{00}, as shown in Fig. 2(f) and Fig. 3. Moreover, solving cases with various albedos, widths of the irradiation pulse, spatial distributions of irradiation, aspect ratios and optical sizes, we find that similar M_{00} distributions always occur at large time, provided that the 2-D finite medium is scattering and its MFPS is much larger than the characteristic geometric size of the medium [12]. Here, the characteristic geometric size is the largest length characterizing the medium. For example, if $z_0 < r_0$ then r_0 is the characteristic

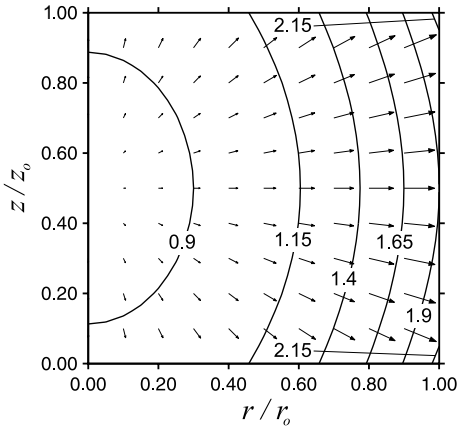

Fig. 3. The spatial distribution of $[M_{00}(r,z,t)/I_0] \times 10^{13}$ and the directions of radiative fluxes at $ct/z_0 = 10.0$ for the case with $\beta r_0 = \beta z_0 = 0.1$ and $\omega = 1.0$ (arrow: the direction of radiative flux at the arrow beginning point).

geometric size of the medium. When the MFPS of the medium considered is not far larger than the characteristic geometric size of the medium, the distribution of M_{00} for transient radiative transfer is similar to time-independent radiative transfer [13]. That is, the M_{00} of medium core is larger than the M_{00} of the medium in the border. Results of an example with $\omega = 1.0$ and a moderate MFPS is shown in Fig. 4. For convenience of interpretation, in Figs. 3 and 4, directions of the radiative fluxes and contour of M_{00} are shown together. From Figs. 3 and 4, it is found that directions of the radiative flux and the gradient of M_{00} for the case with an MFPS much larger than the characteristic geometric size of the medium are almost the same and those for the case with

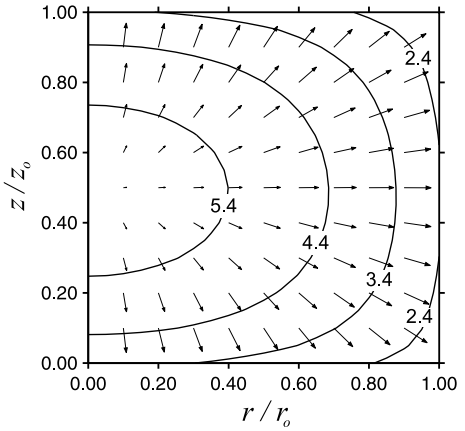

Fig. 4. The spatial distribution of $[M_{00}(r,z,t)/I_0] \times 10^3$ and the directions of radiative fluxes at $ct/z_0 = 4.0$ for the case with $\beta r_0 = \beta z_0 = 1.0$ and $\omega = 1.0$ (arrow: the direction of radiative flux at the arrow beginning point).

an MFPS not much larger than the characteristic geometric size of the medium are almost reverse. The extraordinary distribution of M_{00} for the case with an MFPS much larger than the characteristic geometric size of the medium demands physical interpretation.

When the σ_s of the 2-D medium under consideration is small, radiation (or photons) can travel a very long distance along a direction in the medium before being scattered. The distance is characterized by the MFPS. Thus, if the MFPS is much larger than the characteristic geometric size of the medium, radiation can easily escape from the non-participating boundary of the medium, and so the radiative energy left within the medium decreases with the passage of time at a very large rate. Next, as indicated by Eq. (6), after the pulse irradiation has passed, the M_{00} at a point (r,z) at an instant is the result of radiation that leaves other points, say (r',z'), in the medium at an earlier instant and arrives at (r,z). The influence of the distance, s, between (r',z') and (r,z) is twofold. First, a larger s results in a larger exponential decay along the path. The second is that a larger s corresponds to a larger radiation scattered at an earlier instant, $t' = t - s/c$. The former reduces the magnitude of the integrand in Eq. (6) and the latter increases that in Eq. (6). Besides, to obtain the M_{00} from Eq. (6), we have to integrate not only over the distance but also over all directions, and so the effects of the former and the latter depends on the location of the point of interest. Comparing the distances from the central point $(0, z_0/2)$ to the boundary of the medium and those from a corner point, for example, $(r_0, 0)$, to the boundary, we can find that for the corner point $(r_0, 0)$ there is a region whose inner point has a distance to $(r_0, 0)$ larger than the largest distance from $(0, z_0/2)$ to the boundary. Since the temporal decrease rate of the radiative energy is large and the spatial exponential decay of the radiative intensity is small for the case with an MFPS much larger than the characteristic geometric size of the medium, intensities from a farther region have a significantly large contribution to M_{00}. Therefore, the M_{00} of the medium close to the corner is larger than the M_{00} of the medium around the core, although radiation may escape through the boundary at points around a corner. For convenience, the interesting phenomenon might be called the "temporal-decrease-dominant" phenomenon. The temporal distributions of M_{00} shown in Fig. 5(a) reveal the effect of a large temporal decrease rate on the spatial distribution of M_{00} for the case with $\beta r_0 = \beta z_0 = 0.1$ and $\omega = 1.0$. Each of the curves in Fig. 5(a) reaches the maximum as the peak of the attenuated pulse irradiation arrives at the point of interest and after the instant the M_{00} decreases quickly with the passage of time.

From the point of view of experiment, to measure the radiative fluxes at the boundary is more feasible than to measure the spatial distribution of M_{00} in the medium

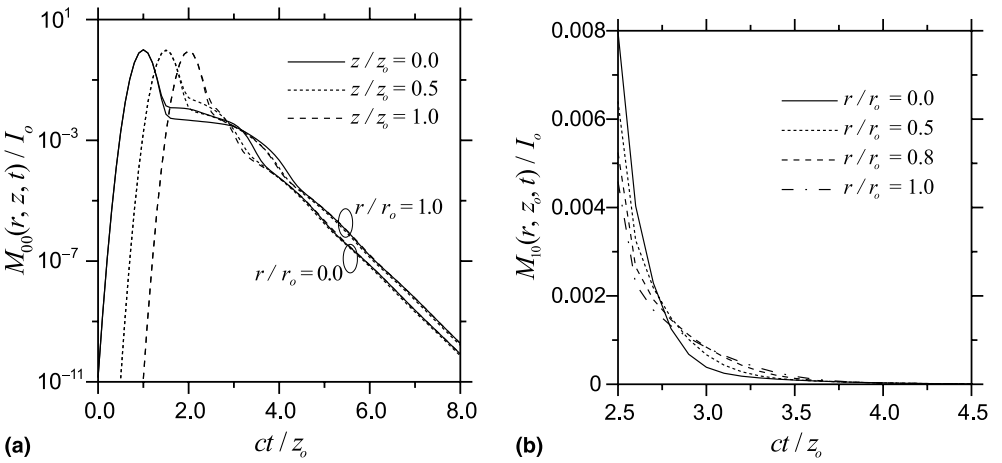

Fig. 5. The temporal distributions of the QM results for the case with $\beta r_0 = \beta z_0 = 0.1$ and $\omega = 1.0$: (a) $M_{00}(r, z, t)$ at various points; (b) $M_{10}(r, z_0, t)$ at various r's.

interior, and so it is beneficial to examine the radiative fluxes leaving the boundary. Four curves of the time-resolved radiative fluxes at different r's on the $z = z_0$ plane for the optically thin problem are plotted in Fig. 5(b). It is about the instant $ct/z_0 = 2.5$ after which the scattering dominates the radiation transfer within the medium. Thus, only parts of the curves after the instant $ct/z_0 = 2.5$ are shown in Fig. 5(b) to examine the behavior of scattered radiation. Before the instant $ct/z_0 = 3.8$ at which the four curves in the figure become indistinguishable, the four curves in Fig. 5(b) cross each other during the period from $ct/z_0 = 2.7$ to $ct/z_0 = 3.0$. The $M_{10}(0, z_0, t)$ is larger and smaller than $M_{10}(r_0, z_0, t)$ before and after the crossing instant, respectively. As shown in Figs. 2(c) and (d), the $M_{00}(0, z_0, t)$ is larger and smaller than the $M_{00}(r_0, z_0, t)$ at $ct/z_0 = 2.5$ and $ct/z_0 = 3.0$, respectively. Thus, temporal distributions of the M_{10} curves represent the time-resolved spatial distribution of M_{00}, and the multiple crossing instants of the curves show that the transition of the spatial distribution of M_{00} is gradual.

One more example exhibiting such a phenomenon is shown in Fig. 6. For the optically moderate medium ($\beta r_0 = \beta z_0 = 1.0$) with $\omega = 0.1$, both the weak scattering and the strong absorption of the medium make the temporal decrease rate of the radiative energy within the medium large enough to result in the temporal-decrease-dominant distribution of M_{00}.

If the optically moderate medium ($\beta r_0 = \beta z_0 = 1.0$) has a larger ω, say, $\omega = 1.0$, then the MFPS of the medium becomes smaller. A photon emanating from the medium core has a larger chance to be scattered before reaching the medium boundary, and so the stronger scattering reduces the radiative transfer from the medium core to the boundary. Then, the temporal decrease rate of the radiative energy becomes smaller, and the contribution of the intensity from a far region becomes comparable with or smaller than that of the intensity from the neighborhood of a considered point. Thus, after the attenuated pulse irradiation has passed through the medium, the M_{00} of the core is larger than the M_{00} of the boundary, and the direction of the radiative flux at a point is nearly the opposite of the gradient of M_{00} at the point, as shown in Fig. 4. Such a spatial distribution of M_{00} is similar to that for time-independent radiative transfer. Moreover, a 2-D finite optically thick medium with a not large MFPS also has a similar spatial distribution of M_{00} at large time. To save space, the spatial distribution of M_{00} for the optically thick medium is not shown here.

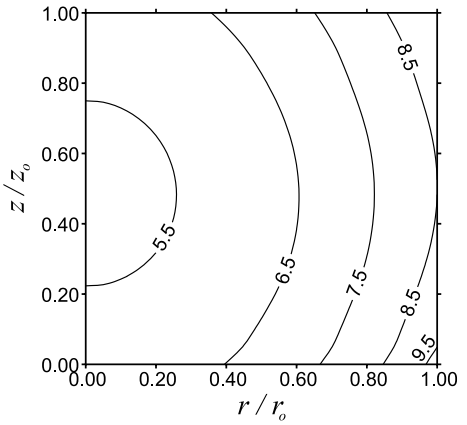

Fig. 6. The spatial distribution of $[M_{00}(r, z, t)/I_0] \times 10^7$ at $ct/z_0 = 4.5$ for the case with $\beta r_0 = \beta z_0 = 1.0$ and $\omega = 0.1$.

The transient radiative transfer in 2-D finite cylindrical media of the fixed aspect ratio $z_0/r_0 = 1.0$ with various combinations of β and σ_s may be classified into groups according to their types of the spatial distribu-

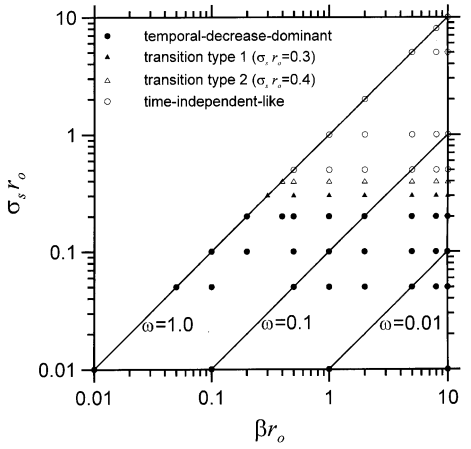

Fig. 7. The map for various spatial distribution types of $M_{00}(r,z,t)$ at large time in 2-D finite media with $z_0/r_0 = 1.0$.

tion of M_{00} at large time. In Fig. 7, the media which have similar spatial distributions of M_{00} at large time are indicated by the same symbol. As shown in Fig. 7, whether the spatial distribution of M_{00} is temporal-decrease-dominant or time-independent-like depends strongly on the MFPS $= 1/\sigma_s$ and seems to be independent of the absorption coefficient, $\kappa = \beta - \sigma_s$, for a wide range of optical sizes. The temporal-decrease-dominant phenomenon occurs when $\sigma_s r_0 \leqslant 0.2$, while the time-independent-like distribution of M_{00} appears when $\sigma_s r_0 \geqslant 0.5$. As the value of $\sigma_s r_0$ varies from 0.2 to 0.5, the spatial distributions of M_{00} at large time show transition types between the temporal-decrease-dominant and the time-independent-like distributions. Examples for transition from the temporal-decrease-dominant distribution to the time-independent-like distribution have been shown in [12], and only one of them is plotted in Fig. 8.

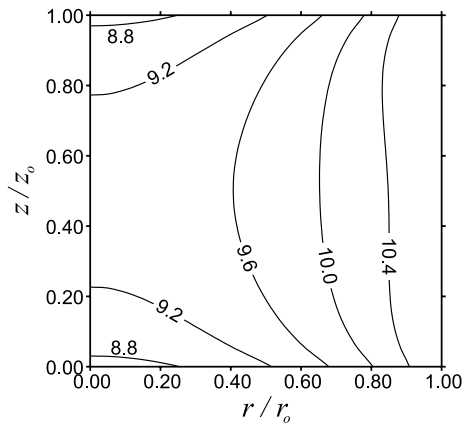

Fig. 8. The spatial distribution of $[M_{00}(r,z,t)/I_0] \times 10^8$ at $ct/z_0 = 6.0$ for the case with $\beta r_0 = \beta z_0 = 1.0$ and $\omega = 0.3$ (an example of transition type 1).

The results in [12] (or Figs. 2(f), 6 and 8) clearly show that the transition is a continuous change with varying $\sigma_s r_0$. It is noted that the above sorting of the spatial distributions of M_{00} at large time in Fig. 7 is not strict, because the transition is not abrupt. Besides, we also find that the media with an identical value of $\sigma_s r_0$ not only have similar spatial distributions of M_{00} at large time, but also have similar time-resolved evolution of the spatial distribution types of M_{00}. This is because the radiation propagation is governed by the scattering and the geometric size of the medium. Two sets of figures showing similar evolution of the two media with the same value of $\sigma_s r_0$ have been given in [12]; they are not duplicated here to save space.

4. Concluding remarks

Transient radiative transfer in 2-D finite cylindrical scattering media is considered. The exemplified problems are solved by the QM, and the RMCM is also adopted to solve problems to validate the QM results. Comparisons of the results by the two methods show that the QM solutions based on the exact integral equation formulation are effective and are of high accuracy.

As shown by the results, for the transient radiative transfer in a 2-D finite cylindrical medium with a large MFPS the radiative energy near the boundary is more than that in the core of the medium, after the attenuated pulse irradiation has passed through the medium. Such a spatial distribution of the radiative energy for the above transient case at large time is just distinct from those of the other transient cases and time-independent radiative transfer. It may be concluded that the influence of the decrease rate of the radiative energy with the passage of time is larger than that of the extinction decay of the radiative intensity along a propagation path for the transient radiative transfer in a 2-D finite medium with a larger MFPS than its geometric size, and that $\sigma_s r_0$ is the major factor in determining the temporal evolution of the spatial distribution type of the radiative energy.

Acknowledgements

This work is supported by the National Science Council of the Republic of China in Taiwan through the Grant NSC 89-2212-E006-051.

References

[1] Y. Yamada, Light-tissue interaction and optical imaging in biomedicine, in: C.L. Tien (Ed.), Annual Review of Heat Transfer, vol. 6, Begell House, New York, 1995 (Chapter 1).

[2] M.Q. Brewster, Y. Yamada, Optical properties of thick, turbid media from picosecond time-resolved light scattering measurements, Int. J. Heat Mass Transfer 38 (1995) 2569–2581.
[3] K. Mitra, S. Kumar, Development and comparison of models for light-pulse transport through scattering-absorbing media, Appl. Optics 38 (1999) 188–196.
[4] E.A. Bucher, Computer simulation of light pulse propagation for communication through thick clouds, Appl. Optics 12 (1973) 2391–2400.
[5] C.-Y. Wu, Propagation of scattered radiation in a participating planar medium with pulse irradiation, J. Quant. Spectrosc. Radiat. Transfer 64 (2000) 537–548.
[6] C.-Y. Wu, S.-H. Wu, Integral equation formulation for transient radiative transfer in an anisotropically scattering medium, Int. J. Heat Mass Transfer 43 (2000) 2009–2020.
[7] A. Ishimaru, Wave Propagation and Scattering in Random Media, Academic Press, New York, 1978.
[8] P.P. Ho, P. Baldeck, K.S. Wong, K.M. Yoo, D. Lee, R.R. Alfano, Time dynamics of photon migration in semiopaque random media, Appl. Optics 28 (1989) 2304–2310.
[9] T.H. Pham, T. Spott, L.O. Svaasand, B.J. Tromberg, Quantifying the properties of two-layer turbid media with frequency-domain diffuse reflectance, Appl. Optics 39 (2000) 4733–4745.
[10] D.M. O'Brien, Accelerated quasi Monte Carlo integration of the radiative transfer equation, J. Quant. Spectrosc. Radiat. Transfer 48 (1992) 41–59.
[11] D.V. Walters, R.O. Buckius, Monte Carlo methods for radiative heat transfer in scattering media, in: C.L. Tien (Ed.), Annual Review of Heat Transfer, vol. 5, CRC Press, Boca Raton, 1994 (Chapter 3).
[12] S.-H. Wu, A study on transient radiative heat transfer by solving integral equations and Monte Carlo simulation, Ph.D. Thesis, National Cheng Kung University, Tainan, Taiwan, ROC, 2000 (in Chinese).
[13] P.-F. Hsu, Z.-M. Tan, S.-H. Wu, C.-Y. Wu, Radiative heat transfer in finite cylindrical homogeneous and nonhomogeneous scattering media exposed to collimated radiation, Numer. Heat Transfer A 35 (1999) 655–679.